ELSEVIER

International Journal of Heat and Fluid Flow 22 (2001) 552–560

International Journal of HEAT AND FLUID FLOW

www.elsevier.com/locate/ijhff

A model for steam bubble formation at a submerged nozzle in flowing subcooled water

W.B. Chen, Reginald B.H. Tan *

Department of Chemical and Environmental Engineering, National University of Singapore, 10 Kent Ridge Crescent, Singapore 119260, Singapore

Received 6 June 2000; accepted 10 April 2001

Abstract

A non-spherical model for bubble formation coupled with phase change at a submerged nozzle in a flowing subcooled liquid is presented. The interface element approach is applied to describe the dynamics of bubble formation. The bubble is assumed to be surrounded by a thin thermal boundary layer, in which the saturated steam condenses partially as the bubble grows. The effect of a parallel flowing liquid is taken into account by pressure analysis of surrounding liquid. The results computed from present model are compared with the experimental data in the literature as well as with the results computed from other models. The results are in good agreement and show a significant improvement over other models.

Keywords: Steam bubble formation; Nozzle; Momentum transfer; Heat transfer; Phase change; Mathematical modeling

1. Introduction

In order to enhance the rate of transport between the phases in many direct contact heat and/or mass exchange processes, a condensable gas is often injected into a liquid through a submerged orifice or nozzle. When the liquid temperature is below saturation, i.e., subcooled, some condensable vapor would condense at the interface during bubble growth. It is therefore of interest to investigate both the dynamics and transfer phenomena of a vapor bubble formation in a subcooled liquid.

Gas bubble formation at a submerged orifice without accompanying heat and mass transfer at the bubble interface has been extensively studied both experimentally and theoretically. Also, considerable research has been done on vapor bubble growth in a boiling process. A recent comprehensive review of these two subjects has been undertaken by Sadhal et al. (1997). However, few reported investigations have been published on the combined effects of these two basic phenomena on the vapor bubble in a subcooled liquid.

Denekamp et al. (1972) and Cho and Lee (1990) have reported models of steam bubble formation at a nozzle in a flowing liquid. In general, these models have assumed the bubble to be spherical, i.e., its geometry is completely described by its radius and by the height of its center above the orifice. Two equations, one governing radial growth, the other governing vertical translation were formulated to compute the bubble growth. However, experimental results have shown that bubble shapes during formation are generally non-spherical. Typically, a bubble starts off as a hemisphere, then becomes approximately spherical as it expands, and finally attains the shape of an irregular ellipsoid with a neck. Moreover, both Denekamp et al. (1972) and Cho and Lee (1990) employ artificial detachment criteria to determine the termination of bubble formation.

The objective of the present work is to study theoretically steam bubble formation at a single submerged nozzle in subcooled parallel flowing water. A realistic non-spherical model for bubble formation coupled with phase change is described. The model attempts to calculate the instantaneous shape of the steam bubble during its formation and to determine the bubble size at detachment, frequency of bubble formation, total steam flow rate as well as steam condensing rate. The effects of flowing liquid velocity, total temperature difference between injected steam and the subcooled liquid will be discussed.

2. Model development

The system under investigation consists of saturated steam that is injected vertically upwards at pressure P_c (or temperature T_c) through a nozzle submerged in subcooled water (bulk temperature $T_{\ell b}$) of depth h. The water flows upward at a velocity v_0 parallel to the nozzle axis. The steam flow rate is controlled by the pressure drop between the injected steam and the bubble.

The non-spherical bubble formation model proposed by Tan and Harris (1986) is modified to calculate the movement of the interface elements in parallel flowing water. This approach assumes instantaneous bubble shape is axial symmetry

* Corresponding author. Tel.: +65-874-6360; fax: +65-779-1936.
E-mail address: chetanbh@nus.edu.sg (R.B.H. Tan).

0142-727X/01/$ - see front matter
PII: S0142-727X(01)00112-6

Notation

A_b	surface area of steam bubble, m^2
C_1	orifice constant, dimensionless
C_2	steam condensation coefficient, dimensionless
C_p	pressure coefficient defined in Eq. (16) and Fig. 2(a), dimensionless
g	acceleration due to gravity, m/s^2
h	height of liquid above the nozzle tip, m
j	mass flux condensing in boundary layer, $kg/(m^2\ s)$
k	thermal conductivity of liquid, W/(m K)
L	latent heat of evaporation, J/kg
$\overline{m}_i$	differential added mass, kg
M	molecular weight, kg/mol
n	number of interface elements
P_b	vapor pressure of bubble, Pa
P_c	injected steam pressure, Pa
P_ℓ	liquid pressure distribution on bubble surface, Pa
P_s	system pressure, Pa
P_0	liquid pressure at infinity, Pa
ΔP	pressure difference between bubble pressure and liquid pressure at interface, Pa
q	volumetric flow rate of steam through orifice, m^3/s
r	fixed cylindrical radial coordinate from axis of bubble, m
r'	virtual cylindrical radial coordinate from axis of bubble, m
r_c	radial coordinate measured from centroid of bubble, m
R	equivalent radius of irregular bubble (based on equivalent spherical volume), m
R_a	equivalent radius of irregular bubble (calculated to give the same area with a circular cross-section), m
R_g	gas constant, J/(mol K)
R_0	nozzle radius, m
S	cross-sectional area of bubble envelope, m^2
t	bubble growth time, s
T_b	vapor temperature of bubble, K
T_c	injected steam temperature, K
T_ℓ	liquid temperature within boundary layer, K
$T_{\ell b}$	bulk liquid temperature, K
$T_{\ell R}$	liquid temperature at bubble interface, K
$U_{r'}$	horizontal velocity of element based on virtual coordinate, m/s
$U_{z'}$	vertical velocity of element based on virtual coordinate, m/s
v_0	upward velocity of bulk liquid, m/s
$v_{\ell r}$	radial velocity of liquid, m/s
V_i	volume of liquid displaced by the element since the beginning of its movement, m^3
V_b	steam bubble volume, m^3
z	fixed axial coordinate from orifice (nozzle) horizontal level, m
z'	virtual axial coordinate from orifice (nozzle) horizontal level, m
z_c	axial coordinate of bubble centroid, m
Greeks	
α	added mass coefficient, dimensionless
α_ℓ	thermal diffusivity of liquid, m^2/s
β	angle defined in Eq. (3)
δ	thickness of thermal boundary layer, m
θ_i	angle defined in Fig. 2(a)
ρ_b	density of vapor inside bubble, kg/m^3
ρ_c	density of injected steam, kg/m^3
ρ_ℓ	density of liquid, kg/m^3
σ	surface tension, N/m
φ_ℓ	non-gravitational liquid pressure on bubble surface, Pa
φ_0	non-gravitational liquid pressure at infinity, Pa

and divides the bubble surface into a finite number of small elements. Each element is assigned an added mass that corresponds to the mass of liquid displaced. The instantaneous coordinates of the interface elements at each timestep are calculated by numerical solution of the equations of motion for each element over a small time increment.

Saturated steam is assumed to condense only within the thermal boundary layer, with the temperature at the bubble interface assumed to be in equilibrium with the vapor within the bubble. Following Denekamp et al. (1972), we assume a quadratic temperature profile within the thermal boundary layer. Heat transfer is accounted for by an energy balance equation for the boundary layer.

The effect of a parallel flowing liquid is modeled theoretically by pressure analysis of surrounding liquid. A pressure correction term corresponding approximately to the experimental pressure distribution around a sphere in a steady, laminar, uniform and axisymmetric flow is applied to each element on the bubble surface.

2.1. Basic equations

Assuming an inviscid liquid, each element at the bubble interface moves as a result of forces due to pressure difference and surface tension. In dynamic formation the resultant of these forces is equal to the rate of change in the liquid momentum, assuming that the gas momentum is negligible. And the momentum of the liquid may be calculated using the "added mass" concept and the velocity of the interface. Thus, a force balance at each element generates a set of differential equations of motion in cylindrical coordinates:

$$r'\Delta P\,\mathrm{d}r' - \sigma\,\mathrm{d}(r'\mathrm{Sin}\beta) = \frac{\mathrm{d}}{\mathrm{d}t}(U_{z'}\overline{m})_i, \tag{1}$$

$$r'\Delta P\,\mathrm{d}z' + \sigma\left[\mathrm{d}(r'\mathrm{Cos}\beta) - \frac{\mathrm{d}z'}{\mathrm{Sin}\beta}\right] = \frac{\mathrm{d}}{\mathrm{d}t}(U_{r'}\overline{m})_i, \tag{2}$$

where r', z' are virtual radial coordinate from axis of the bubble and axial coordinate from nozzle horizontal level, respectively, as shown in Fig. 1(a), ΔP is the pressure difference between bubble pressure P_b and the liquid pressure P_ℓ at each interface element. β is an angle defined by

$$\beta = \tan^{-1}\frac{\partial z'}{\partial r'}. \tag{3}$$

The term $\overline{m}_i$ is the differential added mass

$$\overline{m}_i = (\alpha\rho_\ell + \rho_b)V_i, \tag{4}$$

where α is the added mass coefficient, taken as 0.5, and this is regarded to be an average value during the whole formation process, V_i is the volume of liquid displaced by the element since the beginning of its movement. This simplified approach has been successfully applied by Tan and Harris (1986), Liow and Gray (1988) and Wilkinson and van Dierendonck (1994). The detailed procedure proposed by Tan and Harris (1986) is adopted to calculate the differential added mass.

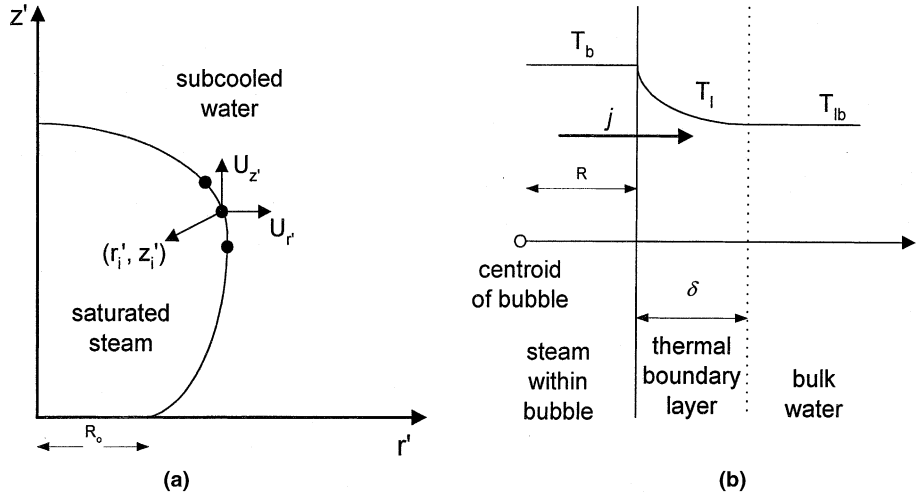

Fig. 1. Physical model of the steam bubble formation: (a) non-spherical growth; (b) heat transfer through the thermal boundary layer.

To account for a parallel flowing liquid with upward velocity v_0, the apparent vertical translation of each interface element, dz'/dt, is defined relative to the uniform liquid velocity v_0. The relationship between the virtual coordinates r', z' and the fixed cylindrical coordinates r, z yields (Terasaka et al., 1999)

$$\frac{dz'}{dt} = \frac{dz}{dt} - v_0 \tag{5}$$

and

$$\frac{dr'}{dt} = \frac{dr}{dt}. \tag{6}$$

The total mass balance for the vapor inside the bubble is

$$\frac{dV_b\rho_b}{dt} = \rho_c q - jA_b, \tag{7}$$

where V_b, A_b are the volume and surface area of bubble, respectively, j is the mass flux of steam condensing within the boundary layer and

$$q = C_1\pi R_0^2\sqrt{\frac{P_c - P_b}{\rho_c}}, \tag{8}$$

where C_1 is the experimentally measured orifice constant.

The energy balance equation appropriate for the liquid phase is

$$\frac{\partial T_\ell}{\partial t} + v_{\ell r}\frac{\partial T_\ell}{\partial r_c} = \frac{\alpha_\ell}{r_c^2}\frac{\partial}{\partial r_c}\left(r_c^2\frac{\partial T_\ell}{\partial r_c}\right), \tag{9}$$

where r_c is the radial coordinate from the centroid of the bubble, $v_{\ell r}$ is the radial velocity of liquid, T_ℓ is the liquid temperature and α_ℓ is the thermal diffusivity of liquid. Assuming that a quadratic temperature profile exists in the boundary layer and that the thickness of the boundary layer is much smaller than the bubble radius, the above equation can be simplified to yield (Bornhorst and Hatsopoulos, 1967)

$$(T_{\ell b} - T_b)^2\delta^2 R^4 = 12\alpha_\ell\int_0^t (T_{\ell b} - T_b)^2 R^4\, dt, \tag{10}$$

where R is the equivalent spherical radius of a non-spherical bubble defined by

$$R = \left(\frac{3}{4\pi}V_b\right)^{1/3}. \tag{11}$$

Both the thickness of the boundary layer and the mass flux are taken as functions of time only. They are related by the boundary condition, i.e., heat flux continuity at the bubble wall:

$$\frac{2k(T_{\ell b} - T_b)}{\delta} = k\left(\frac{\partial T_\ell}{\partial r_c}\right)_{r_c=R^+} = -jL, \tag{12}$$

where k is the thermal conductivity of the liquid, and L is the latent heat of evaporation. From vapor–liquid equilibrium at the interface, we obtain

$$T_b = T_{\ell R} = T^*(P_b) \quad \text{or} \quad P_b = P^*(T_b) = P^*(T_{\ell R}), \tag{13}$$

where the superscript $*$ indicates equilibrium condition.

The effect of parallel liquid flow (velocity v_0) is estimated via the liquid pressure distribution at the bubble interface as shown in Fig. 2. The centroid, C, of the bubble envelope is located by the expression

$$z_c = \frac{\int_1^n z_i\, dS_i}{S}. \tag{14}$$

For each timestep, the angle θ_i for each interface element i is defined as shown in Fig. 2(a). Although a non-spherical bubble surface experiences velocity and pressure distribution different from the potential flow solution (Ryskin and Leal, 1984a), a related study (Ryskin and Leal, 1984b) concluded that for Reynolds Numbers greater than O(100), the potential flow solution provides a good approximation of the physical situation. Our study of steam bubbles covers Re values predominantly in the range 1000–7600, and therefore justifies the use of the potential flow approximation. Fig. 2(b) shows the values of the pressure coefficient C_p for steady flow around a fluid sphere (Hamielec et al., 1967). The authors provided the steady-state solutions of the Navier–Stokes equations for flow around circulating fluid spheres by using finite-difference methods. Their results showed that the potential flow solution provided a good approximation at the front part of a bubble (Clift et al., 1978). The dashed line is the analytical solution for ideal potential flow, while the solid line was used in present model as a close approximation to the solution of Hamielec et al. (1967). In the present model, C_p is estimated as follows:

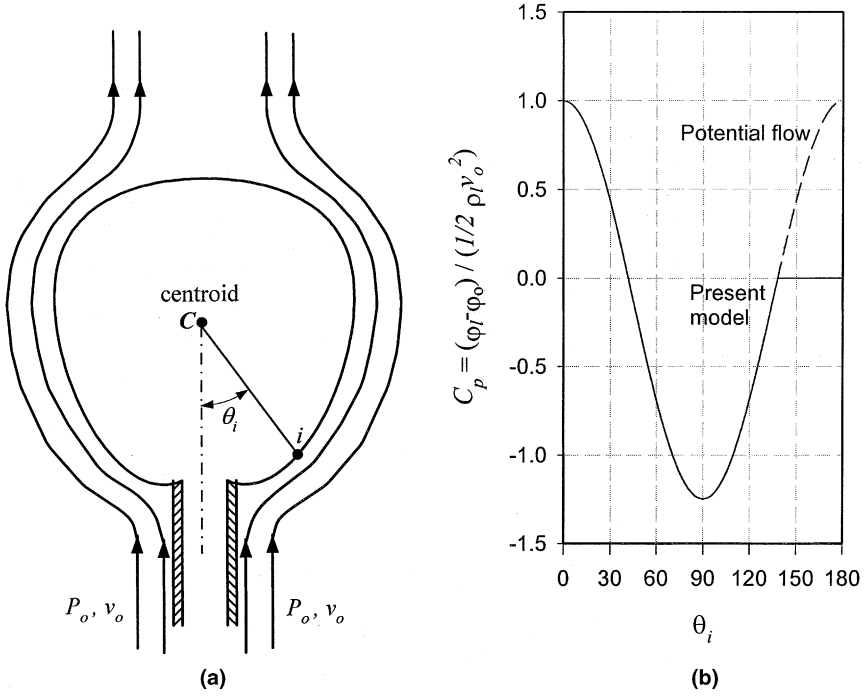

Fig. 2. Analysis of liquid pressure distribution: (a) geometry for estimation of liquid pressure distribution; (b) distribution of dimensionless modified pressure: (– – –) potential flow for spheres and (——) approximation for fluid spheres.

$$C_p = 1 - \frac{9}{4}\sin^2\theta_i, \quad 0 \leqslant \theta_i \leqslant 138.2^\circ, \tag{15a}$$

$$C_p = 0, \quad \theta_i > 138.2^\circ. \tag{15b}$$

Thus, liquid pressure distribution on the surface of bubble can be calculated

$$\varphi_\ell = \varphi_0 + \frac{1}{2}\rho_\ell v_0^2 C_p, \tag{16}$$

where φ_ℓ and φ_0 are non-gravitational pressures with reference to the nozzle tip

$$\varphi_\ell = P_\ell + \rho_\ell g z, \tag{17}$$

$$\varphi_0 = P_0. \tag{18}$$

Therefore, liquid pressure distribution can be computed by

$$P_\ell = P_0 + \frac{1}{2}\rho_\ell v_0^2 C_p - \rho_\ell g z, \tag{19}$$

where P_0 is the absolute liquid pressure at the nozzle tip

$$P_0 = P_s + \rho_\ell g h - \frac{1}{2}\rho_\ell v_0^2 \tag{20}$$

and P_s is the system pressure above the subcooled liquid.

2.2. Initial and boundary conditions

At the beginning of computation, the bubble shape is assumed to be hemispherical, with its radius equal to that of the nozzle. The steam within the bubble is assumed to be saturated and the liquid temperature at the bubble interface to be instantaneously equal to the temperature of steam within the bubble.

Eqs. (1)–(8), (10)–(15b), (19) and (20) can be solved with the following initial conditions:

$$\begin{gathered} R = R_0, \quad P_b = P_0 + \frac{2\sigma}{R_0}, \quad T_{\ell R} = T_b = T^*(P_b), \\ j = C_2\sqrt{\frac{M}{2\pi R_g}}\left[\frac{P_b}{T_b^{1/2}} - \frac{P^*(T_{\ell b})}{T_{\ell b}^{1/2}}\right], \quad \delta = \frac{2k(T_b - T_{\ell b})}{jL}. \end{gathered} \tag{21}$$

The initial mass condensing rate j is assumed to follow the widely used Hertz–Knudsen equation (Tamir and Hasson, 1971), where C_2 is the condensation coefficient taking values between 0.2 and 1.0. The assumed value of C_2 used in the initial estimation of j does not affect the subsequent simulation in any way for all the cases studied, since heat transfer is controlled by the liquid thermal boundary layer.

For bubble formation at a submerged nozzle, the developing bubble envelope is allowed to extend below the level of the nozzle tip, depending on the balance of forces. The required boundary condition for elements below the nozzle tip is that the radial coordinate shall not be less than the nozzle radius, i.e.,

$$z < 0, \quad r \geqslant R_0. \tag{22}$$

2.3. Numerical solution

An explicit finite difference method proposed by Tan and Harris (1986) is extended to solve the equations of bubble formation. The computational procedure of the basic equations is summarized in the following steps:

1. Initialize all parameters.
2. Increase time by Δt.
3. Substitute Eqs. (5) and (6) into Eqs. (1)–(3) and solve the equations of motion for each element i to yield new true coordinates of each element.
4. Compute the bubble volume and surface area by numerical integration of coordinates of all elements.
5. Apply straightforward Runge–Kutta method to solve Eqs. (7) and (10) simultaneously to obtain the instantaneous

steam condensation rate j (or thickness of boundary layer δ) and pressure of vapor inside the bubble P_b.

6. Compute the liquid pressure distribution P_ℓ at the bubble interface.
7. Return to step 2 and repeat until reach detachment.

Owing to the high initial bubble growth rates coupled with high condensation rates, a very small timestep of 10^{-8} s was used during the computation.

3. Results and discussion

We first verify that the current model can predict the bubble volumes and bubble shapes in a cocurrently flowing liquid without heat transfer. As a preliminary test, model simulation results of single bubble formation in a cocurrently flowing liquid without heat transfer were compared with the experimental data of Terasaka et al. (1999).

The instantaneous bubble volumes and shapes are shown in Fig. 3 for the case of N_2/water, orifice radius $R_0 = 0.595$ mm, chamber volume $V_c = 49.7$ cm^3, gas flow rate $Q = 5.11$ cm^3/s, flowing liquid velocity $v_0 = 8.67$ cm/s. Fig. 3(a) compares the simulated bubble growth rates with the experimental data and shows the prediction results correlate well with experimental data. The corresponding bubble shape obtained by our present model is shown in Fig. 3(b). The time interval between two consecutive contours was 4 ms. The bubble detached when the bubble neck closed. The computed bubble shape agrees with the shape photographed by a high-speed video camera by Terasaka et al. (1999).

Simulations of steam bubble formation in water were performed for experimental conditions corresponding to Denekamp et al. (1972). These conditions are summarized in Table 1.

Fig. 4 shows the simulated bubble growth sequences based on the experimental conditions of runs 3 and 4. The conditions for these two runs were virtually identical except for the liquid flow velocity, which were 0.112 and 0.314 m/s, respectively. The time interval between two consecutive contours is 5 ms, and the final shape shows neck closure and hence detachment. These sequences clearly show the effect of liquid velocity on bubble shapes during formation and detachment time. The bubbles are approximately spherical only in the early stages of formation, eventually becoming noticeably non-spherical and detaching naturally when the neck closes.

The experiments of Denekamp et al. (1972) appear to be based on an unusual tapering nozzle (their nozzle is a 8 mm i.d. Pyrex tube, tapered at its upper end to a small orifice 1.52 mm i.d.), which may cause converging liquid flow above the bubble tip, leading to a rather sharply tapered bubble shape. Similar experiments by other workers using parallel nozzles (for example, Terasaka et al., 1999) reveal the more usual rounded shape at the top, which are closer to our simulated profiles.

The comparison of the bubble growth rate between the results computed by the present model with the experimental data of runs 1 and 3 from Denekamp et al. (1972) is shown in Figs. 5(a) and (b), respectively. The predictions of the spherical models of Denekamp et al. (1972) and Cho and Lee (1990) are also shown in Fig. 5. For presentation of results, an area-equivalent radius R_a (calculated to give the same area with a circular cross-section) is used, following the Denekamp et al.'s interpretation of their experimental data (cf Denekamp et al., 1972). The figure indicates that the results computed by the present model are closer to the experimental data than that by the other two models.

The total mass of steam entering through the nozzle consists of the mass of steam inside bubble and the steam condensed as water. The former can be calculated from the vapor density and volume of bubble at any instant. The latter is equal to the cumulative mass condensed in the boundary layer, and can be computed from the instantaneous steam mass condensing flux j and the surface area of bubble. The average steam flow rate, bubble growth rate and steam condensation rate can be obtained by dividing the total steam mass, bubble mass and steam condensation mass by the time, respectively. Fig. 6 shows the computed total steam mass, bubble mass, condensed mass and average steam flow rate, bubble growth rate, steam condensation rate based on the experimental conditions of run 1 from Denekamp et al. It can be observed that at the beginning of bubble growth, average steam flow rate, steam condensation rate and bubble growth rate increase very rapidly due to the rapid change of temperature in the boundary layer at the beginning of bubble formation.

The six experimental runs from Table 1 were simulated and the results are summarized in Table 2. The experimental data

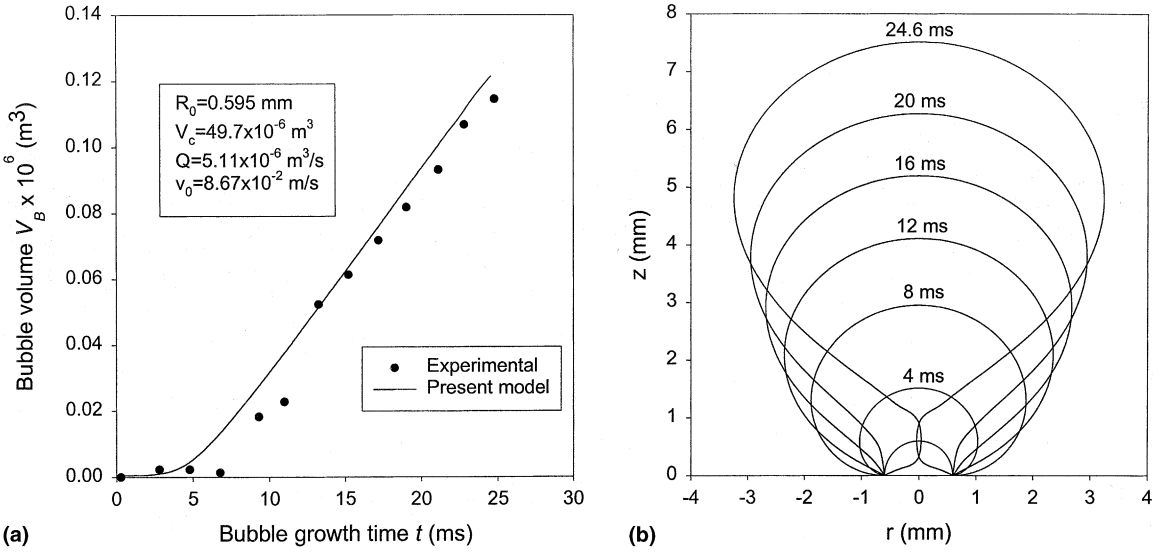

Fig. 3. Simulated bubble growth curve and shapes for bubble formation in a cocurrently flowing liquid without phase change (based on experimental conditions from Terasaka et al. (1999)).

Table 1
Experimental conditions of runs 1–6 from Denekamp et al. (1972)

Run no.	System pressure[a] P_s (Pa)	Liquid height above nozzle h (m)	Water temperature $T_{\ell b}$ (K)	Steam temperature T_c (K)	Flowing water velocity v_0 (m/s)
1	987.94	0.12	323.35	326.05	0.112
2	987.94	0.12	323.35	325.65	0.112
3	983.35	0.12	332.75	334.25	0.112
4	983.40	0.12	332.65	334.15	0.314
5	994.12	0.058	308.05	310.55	0.0762
6	994.15	0.058	307.95	310.45	0.116

[a] System pressure is equal to the saturation pressure of the steam above the bulk water, that is, $P_s = P^*(T_{\ell b})$.

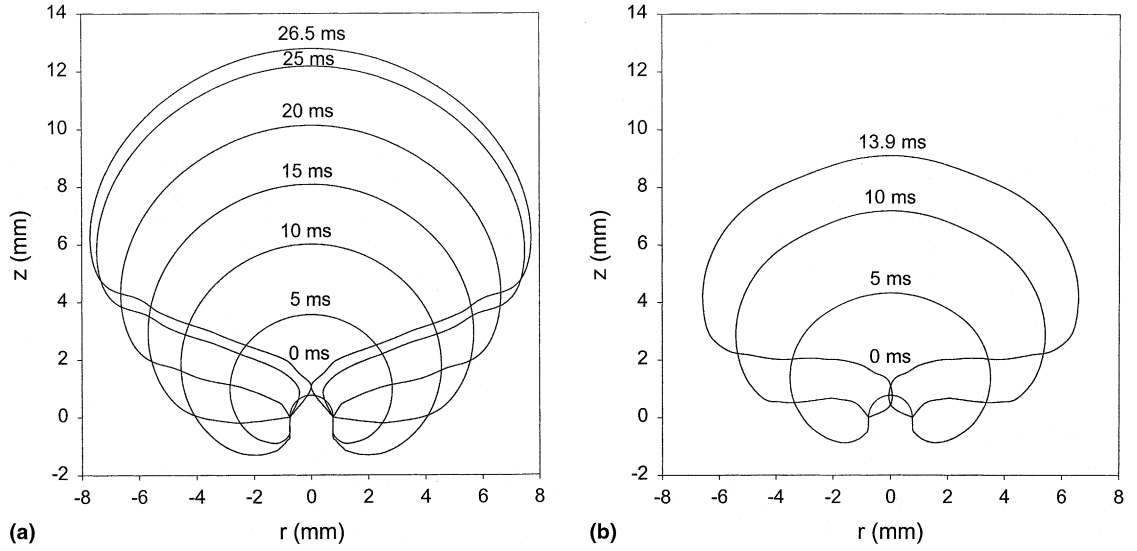

Fig. 4. Computed sequential shapes of steam bubble based on the experimental conditions of runs 3 and 4 from Denekamp et al. (1972): (a) run 3 (Table 1); (b) run 4 (Table 1).

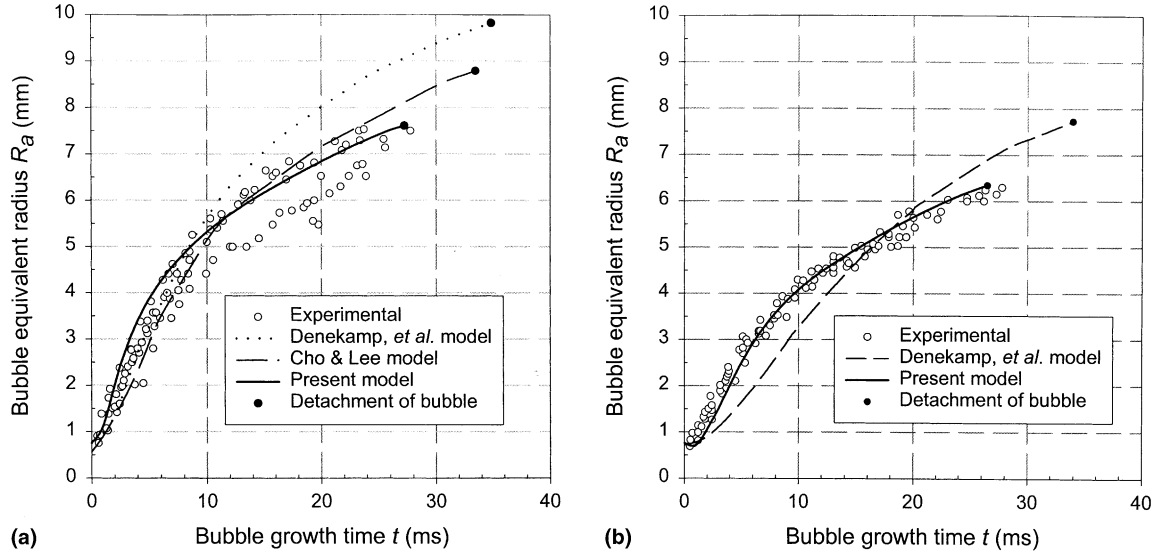

Fig. 5. Computed and experimental values of instantaneous bubble radius: (a) run 1 (Table 1); (b) run 3 (Table 1).

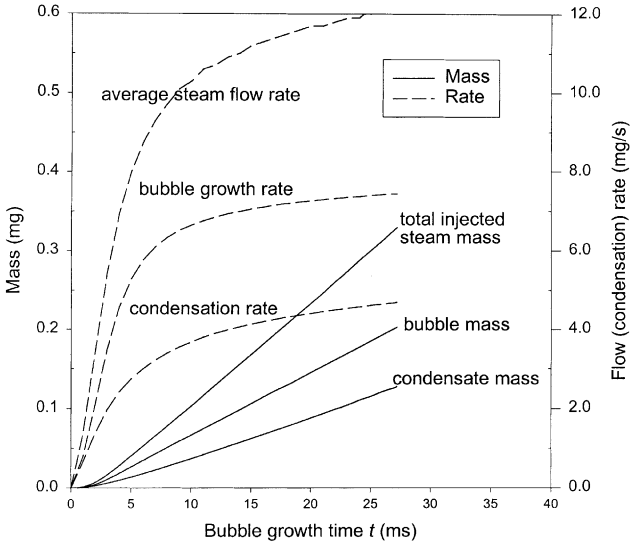

Fig. 6. Computed values of total steam mass, bubble mass, condensed mass and average steam flow rate, bubble growth rate, steam condensation rate based on the experimental conditions of run 1 (Table 1).

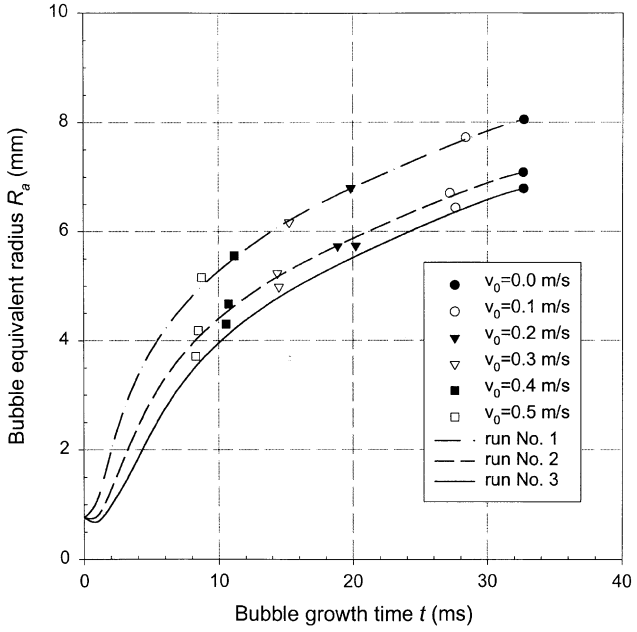

Fig. 7. Computed detachment time and bubble radius at detachment for different liquid flow velocities. Other conditions correspond to runs 1–3 of Table 1.

of bubble radius at detachment, detachment time and the average steam flow rate are compared with the computed results by various models. The present model shows a significant improvement over the other models. Evidently, our present non-spherical model predicts more realistic bubble shapes and consequently a more accurate representation of the heat and mass transfer processes.

Fig. 7 shows the effect of liquid velocity on the instantaneous bubble size. The conditions for the three series of simulations correspond to the conditions of runs 1–3, respectively. The symbols represent the equivalent radius and time at detachment for different liquid flow velocities. Clearly, the instantaneous bubble growth rate is virtually unaffected by the flowing liquid velocity. The main effect of liquid velocity is to affect the detachment time, and thereby the bubble radius at detachment. With increasing of the liquid velocity, the bubble is predicted to detach earlier and the radius at detachment is consequently smaller. This trend was observed experimentally for bubble formation without phase change (Sada et al., 1978; Terasaka et al., 1999).

Fig. 8 shows the effect of total temperature difference on the bubble detachment diameter for bulk liquid temperatures of 37°C and 50°C. Since these experimental data by Denekamp et al. (1972) were not reported with corresponding liquid velocities, two sets of results have been simulated based on the maximum and minimum liquid velocities reported in their work. In Fig. 8, the experimental data can be seen to lie within the range of the two extremes of computed results.

Fig. 9 shows the effect of total temperature difference on the average steam flow rate at various values of bulk liquid temperature. In this series of plots, the liquid velocity used in our model simulations was an average value of 0.2763 m/s, since the corresponding experimental velocities were not reported. It

Table 2
Comparison of computed results with experimental data of Denekamp et al. (1972)

Run no.	Experimental data	Experimental data		Computed results		
				Present model	Cho and Lee (1990)	Denekamp et al. (1972)
1	Detachment time	(ms)	27.2	27.2	32.9	35.0
	Radius at detachment	(mm)	7.5	7.6	8.8	9.8
	Average steam flow rate	(mg/s)	12.17	12.13	11.65	16.33
2	Detachment time	(ms)	27.2	26.3	31.5	32.1
	Radius at detachment	(mm)	4.7	6.6	7.4	8.7
	Average steam flow rate	(mg/s)	8.67	8.48	7.92	10.67
3	Detachment time	(ms)	27.5	26.5	32.4	34.0
	Radius at detachment	(mm)	6.2	6.3	6.8	7.8
	Average steam flow rate	(mg/s)	8.83	8.53	7.76	10.00
4	Average steam flow rate	(mg/s)	8.83	8.63	5.22	8.50
5	Average steam flow rate	(mg/s)	5.00	5.01	4.53	6.33
6	Average steam flow rate	(mg/s)	5.00	4.93	4.40	6.67

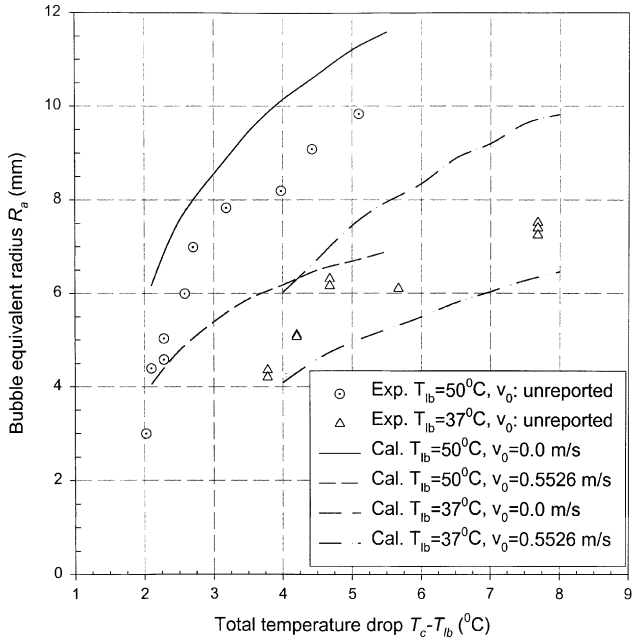

Fig. 8. Effect of the total temperature drop on the bubble detachment size at different bulk liquid temperatures.

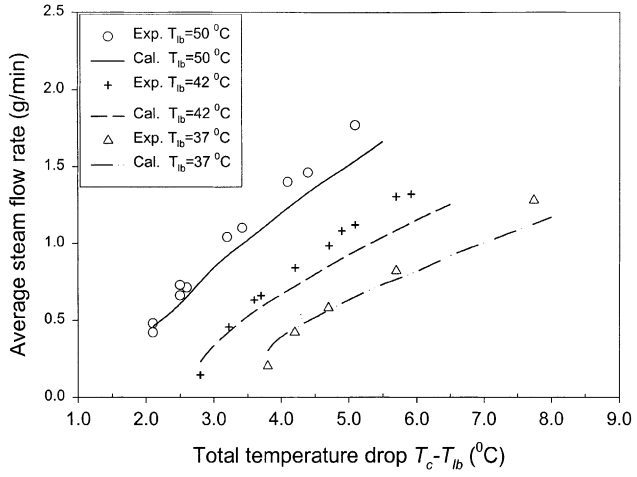

Fig. 9. Effect of the total temperature drop on the average steam flow rate at different steam injection temperatures.

can be seen that the computed average steam flow rates are in good agreement with the experimental measurements by Denekamp et al. (1972).

Fig. 10 shows the effect of total temperature difference on the condensation ratio (the ratio of the condensate mass to the total mass of steam injected during bubble formation and detachment, or the ratio of the average condensation rate to the average steam flow rate), for several values of liquid bulk temperatures and flowing liquid velocities. It indicates the condensation ratio decreases with the increase of the temperature drop, at all values of liquid bulk temperature and liquid velocity studied. The larger the temperature drop is, the bigger the driving force (pressure difference between bubble and the liquid) for bubble formation is. Hence, the bubble size at the detachment is bigger and a deeper liquid layer is needed to condense completely, in case of larger temperature drop,

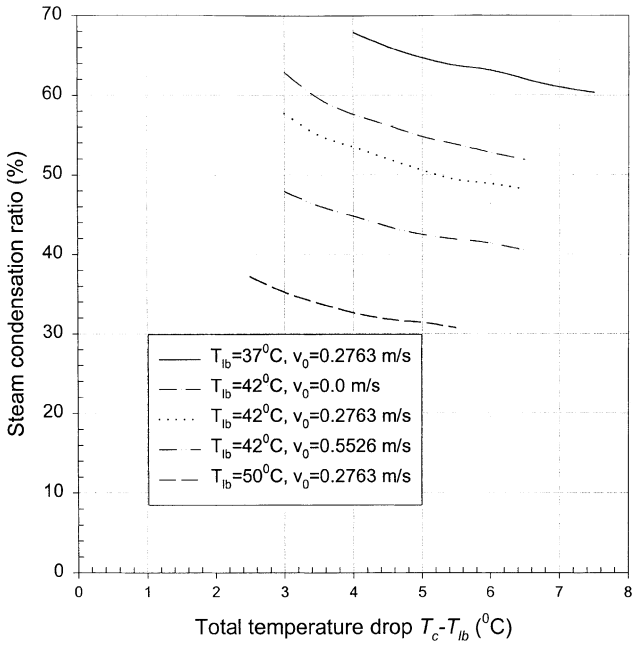

Fig. 10. Effect of the total temperature drop on the steam condensation ratio.

leading to a lower condensation ratio (Cho and Lee, 1990). Concerning the effect of flowing liquid velocity, with the increase of liquid velocity, the bubble is predicted to detach earlier and bubble size is smaller, while the average steam flow rate through the nozzle is almost same. During bubble growth, growth rate is highest in the earlier period of formation, therefore the average condensation rate is lower for higher liquid velocity.

4. Conclusions

An improved model for single steam bubble formation at a submerged nozzle in subcooled flowing water has been developed. The model predicts the instantaneous bubble shape, detachment time, average steam flow rate as well as the steam condensation rate. The simulated results in terms of detachment time, equivalent radius and average steam flow rate are in good agreement with experimental data from Denekamp et al. (1972), and show significant improvement over other theoretical models.

The formation of steam bubbles at a nozzle in subcooled flowing water is an interesting but complex process involving fluid flow and heat and mass transfer. The results of our model show that a significant proportion of steam condensation (typically 30–70%) occurs during the formation process. The model results also show a decrease in steam condensation ratio with increase in subcool, indicating a dominance of inertial and buoyancy effects over heat transfer effects. The effect of increased liquid velocity is to accelerate bubble detachment, leading to lower condensation ratio.

The interfacial element method with an overall average added mass coefficient appears to successfully model the physical phenomena of fluid flow and heat transfer. In particular, the model generates realistic bubble shapes during formation and subsequent detachment, and provides a better representation of the condensation and heat transfer processes occurring at the bubble interface.

References

Bornhorst, W.J., Hatsopoulos, G.N., 1967. Bubble-growth calculation without neglect of interfacial discontinuities. J. Appl. Mech., ASME Trans. 89, 847–853.

Cho, S.C., Lee, W.K., 1990. A model for steam bubble formation at a submerged orifice in a flowing liquid. J. Chem. Eng. Jpn. 23 (2), 180–185.

Clift, R., Grace, V.R., Weber, M.E., 1978. Bubbles, Drops, and Particles. Academic Press, New York, pp. 129.

Denekamp, J., Kogan, A., Solan, A., 1972. On the condensation of an injected vapor bubble in a subcooled liquid stream. Prog. Heat Mass Transfer 6, 179–194.

Hamielec, A.E., Johnson, A.I., Houghton, W.T., 1967. Numerical solution of the Navier–Stokes equation for flow past spheres: Part II. Viscous flow around circulating spheres of low viscosity. AIChE J. 13, 220–224.

Liow, J., Gray, N.B., 1988. A model of bubble growth in wetting and non-wetting liquids. Chem. Eng. Sci. 43 (12), 3129–3139.

Ryskin, G., Leal, L.G., 1984a. Numerical solution of free-boundary problems in fluid mechanics. Part 1. The finite-difference technique. J. Fluid Mech. 148, 1–17.

Ryskin, G., Leal, L.G., 1984b. Numerical solution of free-boundary problems in fluid mechanics. Part 3. Bubble deformation in an axisymmetric straining flow. J. Fluid Mech. 148, 37–43.

Sada, E., Yasunishi, A., Katoh, S., Nishioka, M., 1978. Bubble formation in flowing liquid. Can. J. Chem. Eng. 56, 669–672.

Sadhal, S.S., Ayyaswamy, P.S., Chung, J.N., 1997. Transport Phenomena with Drops and Bubbles. Springer, New York, pp. 311–403.

Tamir, A., Hasson, D., 1971. Evaporation and condensation coefficient of water. Chem. Eng. J. 2, 200–210.

Tan, R.B.H., Harris, I.J., 1986. A model for non spherical bubble growth at a single orifice. Chem. Eng. Sci. 41 (12), 3175–3182.

Terasaka, K., Tsuge, H., Matsue, H., 1999. Bubble formation in cocurrently upward flowing liquid. Can. J. Chem. Eng. 77 (3), 458–464.

Wilkinson, P.M., van Dierendonck, L.L., 1994. A theoretical model for the influence of gas properties and pressure on single-bubble formation at an orifice. Chem. Eng. Sci. 49 (9), 1429–1438.